JACS
JOURNAL OF THE AMERICAN CHEMICAL SOCIETY

ARTICLE

pubs.acs.org/JACS

Smart Polymer Nanoparticles Designed for Environmentally Compliant Coatings

Mohsen Soleimani,[†,‡] Jeffrey C. Haley,[‡] Daniel Majonis,[‡] Gerald Guerin,[‡] Willie Lau,[§] and Mitchell A. Winnik*[,†,‡]

[†]Department of Chemical Engineering, University of Toronto, Toronto, Ontario, Canada M5S 3E5

[‡]Department of Chemistry, University of Toronto, Toronto, Ontario, Canada M5S 3H6

[§]Dow Advanced Materials, The Dow Chemical Company, 727 Norristown Road, Spring House, Pennsylvania 19477, United States

Supporting Information

ABSTRACT: We describe the synthesis, characterization, and film-forming properties of two-component nanoparticles that undergo a reversible morphology transformation in water as a function of pH. The particles consist of a high molecular weight acrylate copolymer and an acid-rich oligomer designed to be miscible with the polymer when its −COOH groups are protonated. Attaching a fluorescence resonance energy transfer (FRET) pair to components inside the nanoparticles enabled us to assess morphology at the molecular level. By inspecting changes in the donor fluorescence decay profile at different pH values, we established miscibility of the components in acidic solution but with charge-induced phase separation when the oligomers were neutralized to their carboxylate form. Complementary titration experiments revealed that the nanoparticles adopt a core−shell structure when the acid groups are deprotonated. We studied the effect of the acid-rich oligomer on the diffusion rate of the high molecular weight polymers following film formation. Our results show that the carboxylated oligomer enhanced the rate of diffusive mixing between high molecular weight molecules by more than 2 orders of magnitude. FRET measurements carried out on partially dried films using a low-resolution microscope showed that the carboxylate oligomer shell can delay coalescence for ca. 30 min after passage of the drying front. This delay is expected to help with increasing the 'open time' of latex paints, a desirable property of solvent-based paints that remains difficult to achieve with (environmentally compliant) waterborne paints. Use of ammonia as a volatile base resulted in synergistic effects: initial retardation of coalescence followed by acceleration of diffusive mixing as the ammonium salts dissociated and ammonia evaporated from the film.

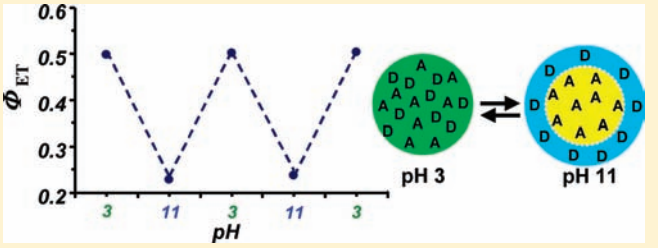

INTRODUCTION

Smart polymers are defined as polymers that sense changes in their environment and respond to these changes in useful ways.[1] Among the stimuli to which polymers can respond are light, temperature or pH changes,[2] or the variation of electrical potential.[3] Materials fabricated from smart polymers are normally targeted for "high technology" applications in areas, such as drug delivery,[4] biotechnology,[5] sensors and optical displays.[6] For systems that operate in solution, one classic example is based upon thermosensitive microgels which undergo a volume phase transition when heated above a critical temperature.[7] Introduction of pH-sensitive functionalities can shift the phase-transition temperature in a way that is pH dependent.[8] These microgels are being developed for drug delivery applications.[9]

Here we describe a new class of colloidal polymer particles that undergo a reversible change in morphology, from a uniform polymer blend to a core−shell structure, upon a change in pH. These particles were designed to provide a new approach to pressing problems with what one might consider a commodity material: water-based (latex) paints. The essential feature of latex paints is that as an aqueous dispersion of polymer nanoparticles dries, the particles fuse to form a continuous transparent and mechanically robust film. This film acts as a binder to support TiO_2 and other pigments on a substrate, providing hiding, color, and protection from the elements. The two issues that these novel latex particles were designed to address are environmental concerns and performance. Environmentally compliant coatings should form films as they dry with formulations that contain little or no volatile organic compounds (VOCs). Soft polymer nanoparticles will do this, but they yield coatings that are tacky to the touch and have poor mechanical properties. This problem is traditionally overcome with volatile plasticizers that are VOC components.

The performance property that remains a serious challenge for latex coatings is commonly referred to as "open time". Open time or "wet edge time" can be defined as the period of time during which a painter can make corrections to the freshly applied wet paint film without leaving brush marks.[10,11] The edges of a paint film are thinner and will dry more rapidly than the bulk of the

Received: April 4, 2011
Published: June 29, 2011

Figure 1. Film formation by soft polymer nanoparticles covered with an oligomeric shell: (a) before the end of water evaporation and (b) after particle deformation. In our design, the shell can act as a temporary barrier to the onset of polymer diffusion across the interparticle boundaries.

film. If the edge is dry and subsequently repainted with a new layer of paint, the dried edge will be visible and cause an irregularity at the paint surface. Solvent-based (e.g., alkyd) coatings are much slower drying than latex coatings, and one has much longer time to rework the edges of a painted area to achieve a smooth and uniform finish. For health reasons, however, and a more general concern for the environment, solvent-based coatings are being replaced by latex paints. Since open time is not easily measured, it is difficult to assess except in a qualitative way. Here we will point to the potential for the new "smart" latex particles to improve the normally short open time of latex coatings.

To achieve these properties we sought a polymer nanoparticle design in which the base latex would have a typical composition for an architectural coating, a relatively high molecular weight (high-M) poly(butyl acrylate-co-methyl methacrylate) [P(BA-MMA)] polymer with a monomer ratio of 55/45 by weight (48.8 mol % BA) with a targeted glass transition temperature (Tg) of 7 °C. These particles would be loaded with a second, low molecular weight, polymer (oligomer) with a much lower Tg. The oligomeric material would contain carboxyl groups in the form of methacrylic acid as well as styrene, methyl methacrylate, and butyl acrylate. The composition is designed to be molecularly miscible with the high-M P(BA-MMA) when the carboxyl groups are protonated but immiscible when they are deprotonated. The styrene units prevent the carboxylate form of the oligomer from dissolving in the aqueous phase. In our design, upon deprotonating acid groups, the oligomer would be neutralized and phase separate from the high-M base polymer to form a core−shell structure with a shell rich in $-COO^{(-)}$ groups. As water evaporates from the particle dispersion and the particles come into contact, we imagine that the carboxylate-rich shell would form a water swollen membrane,[12] as depicted schematically in Figure 1. This membrane would retard the final stages of drying, delay the onset of coalescence, and thereby promote open time. If the counterion were NH_4^+, then the final stages of drying would result in loss of ammonia to the atmosphere, protonation of the surface carboxyl groups, and miscibility of the oligomer with the base polymer. The miscible oligomer should, in turn, plasticize the base polymer and promote the diffusion of high-M polymer across the interparticle boundaries. This is the event at the molecular level that leads to strong interfaces and robust mechanical properties.

In this paper, we tell a story in three parts. First we describe the synthesis of these smart particles and experiments to establish their morphology. Here we find a remarkable and reversible morphology transformation from a core−shell structure in base to a uniform blend in acidic solution. Second, we show that the protonated form of the oligomer does indeed accelerate polymer diffusion in latex films. Finally, we demonstrate that in films formed from these two-component latex nanoparticles neutralized with aqueous ammonia, there is a significant retardation of nanoparticle coalescence, followed by loss of ammonia and enhancement of polymer diffusion rate in the dry film.

RESULTS AND DISCUSSION

The latex particles of interest were synthesized in two steps. We first prepared the high-M P(BA-MMA) core by traditional starved-fed seeded emulsion polymerization in the presence of 0.2 wt % n-dodecanethiol (C_{12}−SH) to obtain gel-free particles with R_h = 55 nm, $M_w \approx$ 100,000, PDI = 2.5, BA/MMA weight ratio of 55/45, 48.8 mol % of BA, and T_g of 6.8 °C. These particles were used as seeds in a starved-fed emulsion polymerization carried out with a mixture of BA (51.2 mol %), MMA (11.8 mol %), styrene (17.2 mol %), methacrylic acid (MAA, 13.9 mol %), C_{12}−SH (5.9 mol %), and methyl-β-cyclodextrin (MeβCD) as described in Table S1 (Supporting Information). The role of MeβCD is to enhance the transport of C_{12}−SH through the aqueous reaction medium.[13] In this way we incorporated into the particles an equal mass (with respect to the core polymer) of oligomer ($M_n \approx$ 2400, PDI = 2.1, and T_g = −24 °C). At the end of the reaction, the particles were purified by dialysis.

We used fluorescence resonance energy transfer (FRET) measurements to assess the miscibility at a molecular level between the core and the oligomer components of the polymer nanoparticles[14] and to monitor the diffusion of the high-M polymer in latex films formed from these nanoparticle dispersions. This required covalent labeling of the core polymer and/or the oligomer with suitable donor (D) and acceptor (A) dyes. For some experiments, the oligomer was labeled with phenanthrene as the donor dye (D-oligo), and the core polymer A-P(BA_{55}M-MA_{45}) was labeled with an *N*,*N*-dimethylaminobenzophenone derivative (NBen) as the acceptor dye. For polymer diffusion experiments in latex films, parallel samples were prepared with the high-M polymer labeled either with Phe or NBen, and the oligomer was left unlabeled. The characteristics of these polymer nanoparticles are presented in Table 1. The recipes used for the syntheses of these samples are collected in Table S1 (Supporting Information).

The overall carboxylic acid content was determined by titration in tetrahydrofuran (Figure S5, Supporting Information). The results showed complete incorporation of MAA into the oligomer. Details of the polymerization and polymer characterization are provided in the Supporting Information.

Morphology Transformation Caused by a Change in pH. For FRET studies of the morphology in the two component polymer nanoparticles, the high-M polymer was labeled with the acceptor dye, and the oligomer was labeled with the donor dye (cf., Table S1, Supporting Information). The particles contain an equal weight of each component. FRET experiments were carried out by exciting the donor dye at 294 nm with a nanosecond pulsed diode and measuring its decay profiles by the single-photon timing technique.[19] In a model latex containing a phenanthrene-labeled oligomer but no dye in the core, the donor fluorescence decay was exponential, with a lifetime τ_D = 43.4 ns, irrespective of the solution pH. In the as-prepared two-component particles, synthesized in the absence of added base, the carboxylic acid groups were primarily in the protonated form. To study the effect of pH on the particle morphology, highly diluted deionized dispersions (ca. 10^{-3} wt % solids) were added to aqueous solutions of NaOH or HCl with the desired pH.

Table 1. Characterization of the Nanoparticle Dispersions Used in This Study

sample	M_n [a]	M_w/M_n	T_g (°C) [b]	R_h (nm) [c]	poly. [d]	solids content wt %
A-P($BA_{55}MMA_{45}$) [e]	41 000	2.5	6.8	55	0.038	38.5
A-P($BA_{55}MMA_{45}$) + D-oligomer [e,f]	—	—	−4.1	68	0.075	39.2
A-P($BA_{55}MMA_{45}$) [e]	43 400	2.8	7.4	54	0.025	38.4
A-P($BA_{55}MMA_{45}$) + oligomer [e,f]	—	—	−3.8	70	0.052	40.1
D-P($BA_{55}MMA_{45}$) [e]	47 400	3.1	7.2	60	0.037	37.3
D-P($BA_{55}MMA_{45}$) + oligomer	—	—	−4.1	70	0.032	40.1
oligomer	2800	2.4	−24.1	58	0.083	34.1

[a] Nominal molecular weights obtained by gel permeation chromatography by reference to polystyrene standards (Figure S1, Supporting Information). Composition was determined by ^1H and ^{13}C NMR (Figures S2 and S3, Supporting Information). [b] Glass transition temperatures taken as the midpoint of the deflection in differential scanning calorimetry measurements. [c] As prepared samples after purification by dialysis. For oligomer-containing samples, the acid groups in the oligomer are in their protonated state. [d] Particle size distribution measured from second cumulant analysis. The absence of small particles in the sample from possible secondary nucleation was monitored by capillary hydrodynamic fractionation chromatography (CHDF, Figure S4, Supporting Information) [e] D- and A- refer, respectively, to polymers labeled with donor (1 mol %) and acceptor dyes. When the oligomer was donor-labeled, the high-M polymer contained 0.3 mol % acceptor dye. When the oligomer was not labeled, the high-M acceptor-labeled polymer contained 0.6 mol % dye. Samples without these prefixes are unlabeled. [f] The oligomer composition was BA (51.2 mol %), MMA (11.8 mol %), styrene (17.2 mol %), MAA (13.9 mol %), and C_{12}−SH (5.9 mol %). The two-component nanoparticles contain a 1:1 weight ratio of high-M polymer and oligomer.

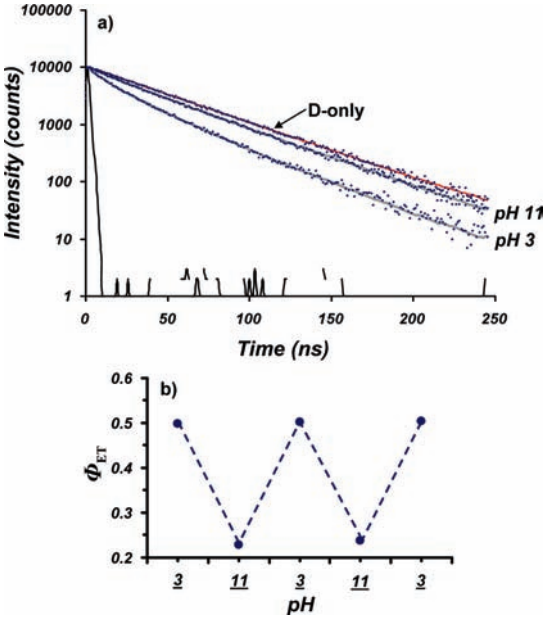

Figure 2. (a) Phe fluorescence decay profiles of the two-component particles at pH of 3.0 and 11.0. The uppermost curve is the exponential unquenched donor decay for a sample with no acceptor dye. (b) Variation of the quantum efficiency of energy transfer (Φ_{ET}) when pH was switched back and forth between acidic and alkaline conditions. The results show that the transition is reversible.

For the initial measurements, a trace of HCl was added to the nanoparticle solution to reduce the pH to 3.0. The donor fluorescent decay curve $[I_D(t)]$ for this dispersion is shown as the lower curve in Figure 2a. Adding NaOH to the dispersion to increase the pH to 11.0 led to an immediate (minutes) and stable change in the $I_D(t)$ decay profile, presented as the upper curve in Figure 2a. The slower but nonexponential donor decay rate for the sample at pH of 11 indicates that some energy transfer takes place in the particles at pH of 11 but much less than in the particles at pH of 3.

Quantum yields of energy transfer Φ_{ET} were calculated via eq 1 from the areas under the normalized donor fluorescence decay curves. In this expression, $I_D^o(t)$ refers to the unquenched donor decay. Details and examples of decay fitting models and results are provided in the Supporting Information.

$$\Phi_{ET} = 1 - \frac{\int_0^\infty I_D(t)\,dt}{\int_0^\infty I_D^0(t)\,dt} \quad (1)$$

Corresponding measurements were carried out at a series of pH values between 3 and 11 (Figure S9, Supporting Information). At pH of 3.0, $\Phi_{ET} = 0.51$, which suggests significant mixing between the two components inside the composite particle. At pH of 11.0, the value of Φ_{ET} decreased to 0.22. As shown in Figure 2b, these changes are reversible. Addition of HCl to reduce the pH to 3 led to an increase in Φ_{ET}, whereas subsequent addition of NaOH to raise the pH back to 11 resulted in a decrease in energy transfer. While Φ_{ET} is fully reversible, each neutralization−reprotonation step increased the ionic strength of the medium, and eventually the nanoparticles precipitated.

The reversibility of the changes in Φ_{ET} (Figure 2b) provides strong evidence that, at high pH, where the carboxyl groups are fully neutralized, the oligomer remains part of the nanoparticle structure. Preliminary experiments with a more hydrophilic oligomer lacking styrene units gave different results: A similar Φ_{ET} value for the initial sample at low pH but incomplete reversibility on successive additions of acid and then base. After centrifugation of this sample at high pH, we observed by UV−vis spectroscopy the presence of soluble donor-labeled material in the supernatant that we attribute to water-soluble oligomer. For the nanoparticles loaded with the styrene-containing oligomer, no water-soluble oligomer could be detected following centrifugation of a latex sample at high pH.

Figure 3a presents the normalized autocorrelation functions measured with 90° dynamic light scattering (DLS) and the corresponding CONTIN plots (Figure 3b) at pH of 3 and 11 for the same samples whose fluorescence decays are shown in Figure 2a. The hydrodynamic radius (R_h) increased from 68 nm at pH of 3

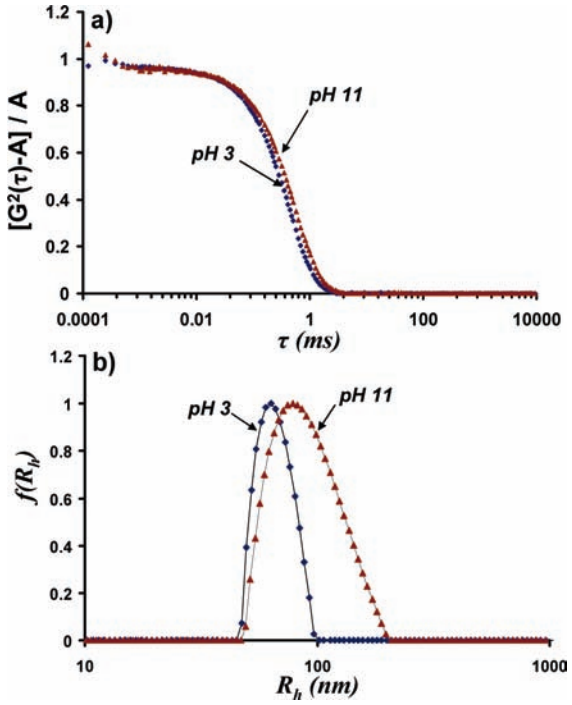

Figure 3. Normalized autocorrelation functions (a) and CONTIN plots (b) from DLS measurements on particles at pH of 3 and 11. From a cumulant analysis, we find that R_h increases from 68 nm at pH of 3 to 78 nm at pH of 11, accompanied by an increase in polydispersity (0.075 at pH of 3; 0.117 at pH of 11).

to 78 nm at pH of 11, corresponding to a ca. 50% increase in particle volume. This swelling is likely a consequence of the osmotic pressure exerted by the mobile counterions.[15,16]

To obtain more information about the particle morphology in acidic and basic solutions, the $I_D(t)$ fluorescence decay profiles of the samples were analyzed in detail. For samples at pH of 3, we fitted the decay profiles to the Förster model (eq 2a) describing a uniform distribution of D- and A- chromophores, consistent with uniform mixing of the two components. In eq 2a, the fitting parameter P is proportional to the molar concentration of acceptor chromophores C_A. N_A is Avogadro's number, τ_D is the donor lifetime in the absence of acceptors (43.4 ns), and R_0 is the Förster radius for the Phe/NBen (2.51 ± 0.04 nm).[17] For a random orientation of immobile chromophores in three-dimensional space, the orientation parameter κ^2 has the value 0.476.[18,19]

$$I_D(t) = A \exp\left[\frac{-t}{\tau_D} - P\left(\frac{t}{\tau_D}\right)^{1/2}\right] \quad (2a)$$

$$P = \frac{4}{3}\pi^{3/2} N_A \left\langle \frac{3}{2}\kappa^2 \right\rangle^{1/2} R_0^{3/2} C_A \quad (2b)$$

$I_D(t)$ decay profiles measured at pH of 3 fit well to eq 2a (Figure S7, Supporting Information), and from the magnitude of P (0.83 ± 0.0015) we calculated C_A = 13.9 mM. This value is close to, but somewhat smaller than, the value C_A = 14.7 mM calculated assuming a uniform acceptor dye distribution and a polymer particle density of 1.12 g/cm^3. This difference can be explained by a small extent of water swelling (5.8 vol %) of the particles. We

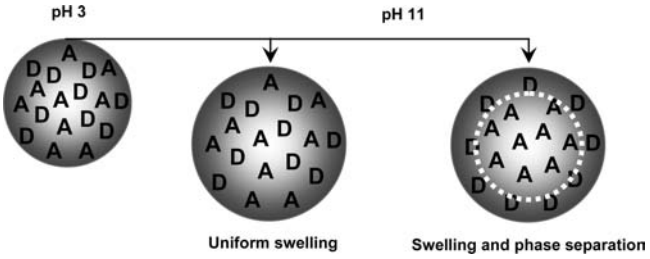

Figure 4. Two possible scenarios (uniform swelling vs swelling accompanied by phase separation) when particles are exposed to alkaline conditions. The particles at pH of 3.0 and 11.0 are drawn approximately to scale.

conclude that at pH of 3 the core polymer and the oligomer components are uniformly and molecularly mixed inside the particle.

Upon ionization of the acid groups, Φ_{ET} decreases, and the particles swell 50% in volume. If the two components remained fully mixed, then the $I_D(t)$ decay profile measured at pH of 11 would still fit to eq 2a but with a reduced P parameter corresponding to C_A = 9.3 mM. The value of Φ_{ET} corresponding to these fitting parameters would be 0.38, which is considerably larger than experimentally obtained value at pH of 11 (0.22). Moreover, decay profiles obtained at pH of 11 do not fit eq 2a. Therefore, the idea of uniform swelling at pH of 11 cannot explain the donor fluorescence decay profile (Figure 4) and the low extent of energy transfer points instead to microphase separation. We attribute the observed changes in Φ_{ET} to a reversible morphology transition from a mixed state (at pH of 3.0) to a charge-induced microphase separation (at pH of 11.0). In other words, a reversible rearrangement of the components occurs as a consequence of deprotonation of COOH groups, which leads to a phase rich in the ionized donor-labeled oligomers that can remix with the acceptor-labeled polymer when the pH is decreased.

While the FRET experiments provide unambiguous evidence for phase separation, these experiments by themselves do not establish a core−shell type morphology for the composite particles. The characteristic length scale sampled in a FRET experiment (on the order of $5R_o$) is sensitive to microphase separation but is too small to distinguish core−shell from other occlusion types of phase separation. To obtain additional information, we took particles equilibrated at pH of 11 and titrated them with acid. Here we found that 74% of the −COOH groups introduced in the oligomer synthesis could be titrated at the particle surface (Figure S6, Supporting Information).[20] We infer from this result that the phase separation at high pH brought most of the acid groups close enough to the surface to be titrated.[21] This suggests the formation of a core−shell structure at alkaline pH. A cartoon showing this morphology change is presented in Figure 4.

Taking the core−shell structure as a model, we carried out a more detailed analysis of the $I_D(t)$ decay profiles measured at pH of 11 to determine the nature of the interface between the hydrophobic polymer core and the carboxylate-rich oligomer shell. This analysis assumes that, as in traditional polymer blends, the concentration profile across the interface between the components can be described by the Helfand−Tagami (HT) model,[22] and the donor and acceptor profiles across the interface follow the segment density profile of the components. For FRET experiments in a spherical geometry, the HT equations for the

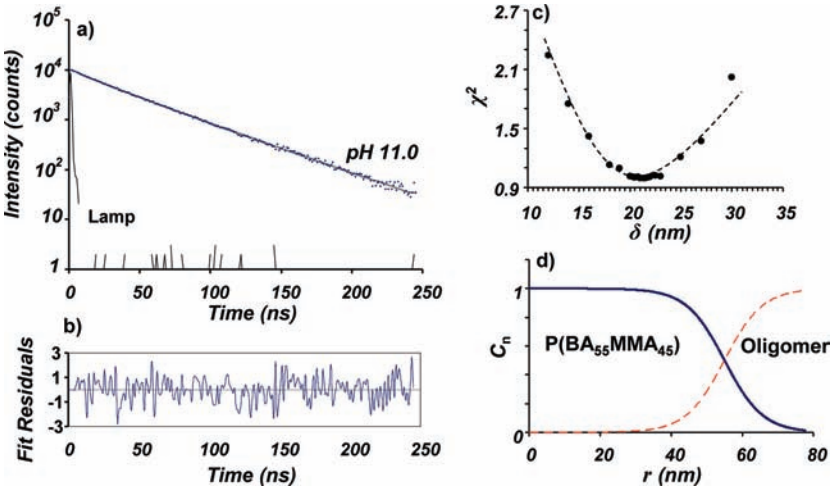

Figure 5. (a) Phe fluorescence decay of the composite particles at pH of 11.0 fitted to a simulated decay obtained based on HT model concentration profile at $\delta = 21 \pm 1$ nm. (b) Weighted residuals of the fit presented in (a), (c) Plot of χ^2 obtained when decays based on various δ were fitted to the experimental decay at pH of 11.0. (d) Plot of normalized radial concentration profile inside composite particle. The solid line represents the high molecular weight component, and the dashed line represents the oligomer concentration.

donor and acceptor can be written as:[23]

$$C_A(r) = (0.5)\{1 + \tanh[2(r - R_s)/\delta]\} \quad (3a)$$

$$C_D(r) = 1 - C_A(r) \quad (3b)$$

Here R_s is the radius of the hydrophobic core, and δ is the interface thickness. $C_A(r)$ and $C_D(r)$ are the local concentrations of acceptor and donor as a function of distance from the center of the particle. To proceed, we carried out simulations to calculate theoretical $I_D(t)$ profiles based upon a Monte Carlo sampling technique that generated concentration profiles according to eq 3, assuming various values of the interface thickness δ. These theoretical profiles were convoluted with the same instrument response function obtained in the experiments. Details are provided in Supporting Information. We then optimized the value of δ to get the best fit of experimental and theoretical decay profiles.

Figure 5a shows the experimental decay profile at pH of 11.0 fitted to a simulated decay profile based on the HT model using a core radius $R_s = 55$ nm for A-P($BA_{55}MMA_{45}$) and a total particle radius at pH of 11 of 78 nm. The best fit is chosen as that in which the weighted residuals appear randomly distributed around zero. The best fit corresponds to a value of 21 ± 1 nm for the interface thickness. This value is confirmed by the deep minimum in the χ^2 vs δ plot presented in Figure 5c. Figure 5d depicts the normalized concentration profile of the oligomer (dashed line) and the high molecular weight component (solid line).

Promotion of Polymer Diffusion by the Acid-Rich Oligomer. To test the ability of oligomer to enhance the diffusion rate of the base latex polymer, we need polymer samples similar to those described above but labeled differently with donor and acceptor dyes. Since we are interested here in the rate of interdiffusion of high molecular weight polymer between adjacent cells formed from latex nanoparticles upon drying, it is the high-M component that needs to be labeled. This requires a pair of essentially identical two-component latex nanoparticle samples, one with the high-M component labeled with Phe as the donor dye, and one with the high-M component labeled with NBen as the acceptor dye. Both samples should contain 50 wt % *unlabeled* oligomer. For comparison purposes, we need a pair of latex samples consisting of D- and A-labeled high-M polymer with no oligomer content. This sample will be used to determine the polymer diffusion rate in the absence of added oligomer.

We synthesized D-P($BA_{55}MMA_{45}$), labeled with 1 mol % of Phe, and A-P($BA_{55}MMA_{45}$), labeled with 0.6 mol % of NBen. These samples were then used to synthesize two-component latex nanoparticles containing 50 wt % of unlabeled oligomer. The high-M D-P($BA_{55}MMA_{45}$) sample was characterized to have $R_h = 60$ nm, $M_n \approx 47\,400$, PDI = 3.1, and $T_g = 7.4$ °C (see Table 1), similar in size, M_n, and polydispersity to the A-P-($BA_{55}MMA_{45}$) sample. Polymer diffusion rates are very sensitive to polymer molecular weight. While it is desirable that the molecular weights of the D- and A-labeled polymer be similar, it is critical that the overall molecular weight of the diffusing species be identical in samples being compared. Thus the two D-labeled components and the two A-labeled components in the oligomer-free and oligomer-containing nanoparticles need to be as identical as possible. This was achieved by using aliquots of the D- and A-P($BA_{55}MMA_{45}$) core particles to study diffusion in the absence of added oligomer. Therefore, the diffusion of the same labeled chains was monitored in both sets of experiments.

To study polymer diffusion in the oligomer-free latex films, we mixed dispersions of the D- and A-($BA_{55}MMA_{45}$) core particles to give a 1:9 particle ratio, spread a few drops on a quartz disk, and allowed the water to evaporate over 30 min in a cold room at 4 °C. In this way we obtained transparent latex films ca. 50 μm thick. The films were prepared in the cold to minimize the amount of interparticle polymer diffusion that might take place as the film dried.[24] Corresponding latex films were prepared from the two-component nanoparticle dispersions. Here we kept the same 1:9 ratio for D- to A-labeled latex nanoparticles. In dried films obtained from this mixture, it can be assumed that each D-labeled nanoparticle is surrounded by A-labeled particles. The acceptor concentration in the films prepared from composite nanoparticles is half of that in films prepared from particles without the oligomers, assuming equal density for the high and low molecular weight components.

Latex films prepared in this way were brought to room temperature (22 °C), and the two different types of latex films

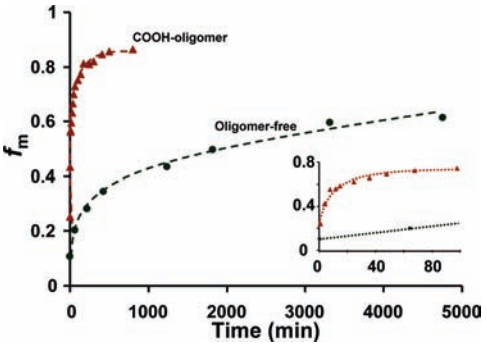

Figure 6. Plots of the extent of mixing f_m as a function of time for latex films formed from D- and A-labeled polymer nanoparticles, comparing films formed from the oligomer-free particles with those formed by the −COOH-containing two-component latex particles.

examined in parallel by donor fluorescence decay measurements as a function of time. $I_D(t)$ decay profiles were analyzed in terms of eq 1 to calculate Φ_{ET} values. Since mixtures prepared in this way differ in acceptor concentration, they cannot be satisfactorily compared in terms of Φ_{ET} evolution. Instead we calculated values of the fraction of mixing f_m, which is defined as fractional growth in Φ_{ET}:

$$f_m(t) = \frac{\Phi_{ET}(t) - \Phi_{ET}(0)}{\Phi_{ET}(\infty) - \Phi_{ET}(0)} \quad (4)$$

Here $\Phi_{ET}(0)$ describes the small amount of FRET across the boundary in a hypothetical film in which D- and A-labeled polymer in adjacent cells are in intimate contact but no polymer diffusion has occurred. Values of $\Phi_{ET}(0)$ can be obtained by simulation.[25] We calculated a value of $\Phi_{ET}(0) = 0.09$ for the oligomer-free latex film and a value of $\Phi_{ET}(0) = 0.06$ for the film containing the COOH−oligomer mixture. Two factors contribute to the larger value for the films formed from the mixture of D- and A-P($BA_{55}MMA_{45}$) polymer nanoparticles. First, there is a higher concentration of A-groups (C_A) in the A-labeled phase. Second, there is a greater interfacial area in films formed by these smaller particles. Experimental values of Φ_{ET} in newly formed films can be larger than these values if some polymer interdiffusion occurs as the wet films dry on the substrate. In Figure 6, the extent of polymer diffusion that took place during film preparation is indicated by values of $f_m(t = 0) > 0$.

$\Phi_{ET}(\infty)$ refers to the final value of the energy transfer quantum efficiency following complete mixing of donors and acceptors. To determine this value, we prepared fully mixed films by solvent casting. A dried latex film was dissolved in a small amount of tetrahydrofuran (THF). The solvent was allowed to evaporate, and the films were annealed at 70 °C in an oven overnight to remove traces of THF. From fluorescence decay measurements on these films we obtained $\Phi_{ET}(\infty) = 0.83$ for the oligomer-free mixture and $\Phi_{ET}(\infty) = 0.70$ for the two-component polymer mixture. The mixture with no oligomer has a higher value of $\Phi_{ET}(\infty)$ because of the higher C_A in this film. These experimental values are close to those obtained from simulations, i.e., 0.87 for the oligomer-free mixture and 0.71 for COOH−oligomer mixture.

In Figure 6, we compare the time evolution of mixing due to polymer diffusion across the interparticle boundaries in the two sets of latex films. The differences are striking. For the oligomer-free film, polymer diffusion at room temperature occurs on a time scale of tens of hours, reaching $f_m = 0.5$ after about 2000 min. In contrast, in the presence of what is admittedly a large amount of COOH−oligomer, polymer diffusion takes place on the time scale of minutes (cf., the inset in Figure 6), reaching $f_m = 0.5$ after about 10 min. In Supporting Information (Figure S8), we present values of calculated apparent diffusion coefficients D_{app} as a function of the extent of mixing. These calculations indicate that the presence of the oligomer in the mixture of D- and A-P($BA_{55}MMA_{45}$) polymer increased the magnitude of D_{app} by 2 orders of magnitude.

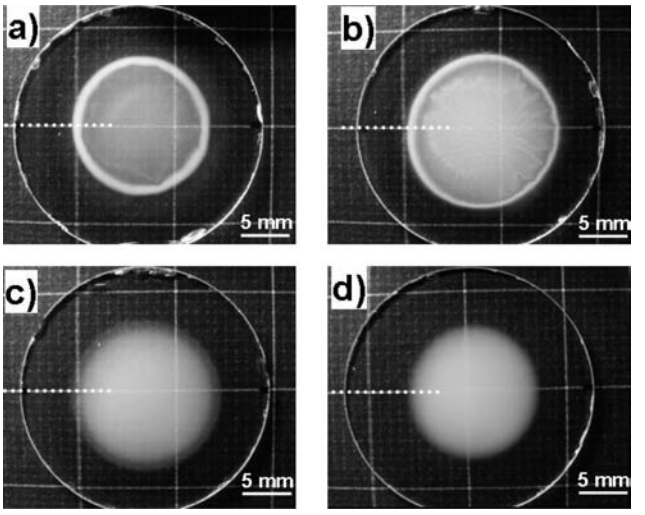

Figure 7. Partially dried latex films containing a mixture of D- and A-labeled polymer nanoparticles after 100 min at 22 °C and 35% RH: (a) Oligomer-free latex; (b) two-component COOH oligomer; (c) two-component latex to which 1 eq $NH_4(OH)$ was added to the dispersion; and (d) two-component latex to which 1 equiv NaOH was added to the dispersion. Fluorescence decay measurements were carried out along the dashed line from the edge of the quartz disk, across the drying front and into the wet (turbid) dispersion.

Retarded Coalescence: The Early Stage of Film Formation at Acidic and Basic pH. In this section, we examine the consequences of changing pH on the earliest stages of film formation for the two-component latex films. For these experiments, we take advantage of our ability to measure fluorescence decay profiles through a low-resolution microscope, with submillimeter resolution, on partially dry latex films. This instrumental setup is described elsewhere.[26] For these experiments, individual mixtures of D- and A-labeled latex nanoparticles were each cast onto a 25 mm diameter quartz disk and allowed to dry at 22 °C and 35% relative humidity (RH). The dispersions dried from the edge inward with the formation of a distinct drying front that separates the transparent dry film from the cloudy center. We used digital photographs to image the drying process. Figure 7 represents images of the four types of partially dried latex films we examined, each allowed to dry for ca. 100 min. As a reference, Figure 7a shows a film of oligomer-free polymer consisting of a mixture of D- and A-P($BA_{55}MMA_{45}$) particles in a 1:9 ratio. The other images are of films of the two-component latex: in (b) with the oligomer in the −COOH form and in (c) and (d) neutralized with one equivalent of NH_4OH and NaOH, respectively.

These images show that a translucent halo followed by a turbid ring separates the wet spot from the transparent dry polymer film for both the oligomer-free latex film (Figure 7a) and the

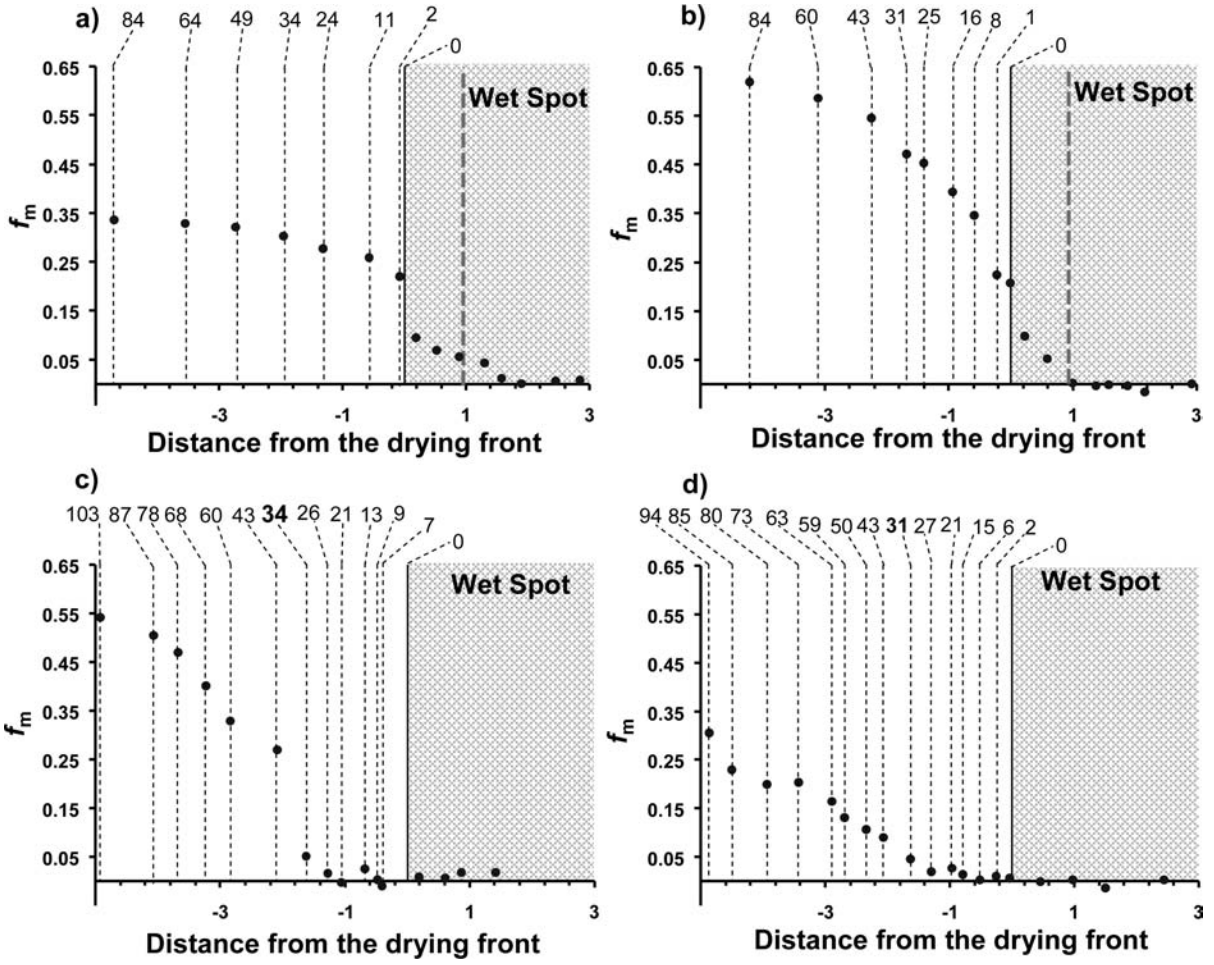

Figure 8. Plots of f_m vs distance from the drying front for the four partially dried latex films presented in Figure 7: (a) oligomer-free film; (b) two-component nanoparticles with −COOH oligomer; (c) two component nanoparticles with the oligomer neutralized with NH_4OH; and (d) two component nanoparticles with the oligomer neutralized with NaOH.

two-component latex in the −COOH form (Figure 7b). This turbid ring appeared after ca. 5 min of drying and advanced concentrically with the drying front as the wet spot contracted. This ring is likely to be a signature of the compaction front identified by Scriven and co-workers.[27] At the compaction front, water has receded from the partially deformed latex particles, creating air voids, which strongly scatter incident light. As the film continues to dry, this foam-like structure collapses into a void-free film. In films neutralized with base, no compaction front can be seen (Figure 7c and d). There is a single boundary (the drying front) between the dry edge and the turbid spot. This boundary formed early on in the drying process and receded inward during drying.

Each film was immediately transferred to a hermetically sealed chamber cooled to 5 °C to stop the drying and to suppress further polymer diffusion. Then donor fluorescence decay measurements were carried out at a series of positions (along the white dotted lines in each image) from the edge of the disk, across the drying front, and into the turbid wet region of the dispersion. $I_D(t)$ profiles were analyzed in terms of eq 1, and f_m values were calculated using eq 4. These values are plotted as a function of the distance from the drying front in Figure 8. In Figure 8a and b, the bold dashed vertical line refers to the compaction front, the inner edge of the bright corona surrounding the wet spot in the middle of the film, and the drying front is chosen as the outer edge of this bright ring, which Scriven has called the coalescence front.[27] The idea behind this term is that coalescence refers to the step in which all hydrophilic material is squeezed out of the interstitial spaces between adjacent cells in a latex film[28] and the polymers in these cells come into contact. Diffusion across a polymer−polymer boundary takes place only after polymer molecules at each side of the boundary come into close contact, a situation described as 'wetting' by Wool.[29]

In Figure 8, the numbers above the thinner dashed lines indicate the time in minutes that had elapsed since the passage of the drying front. Points on the left-hand side of each figure refer to positions in the film that have been dry for the longest times.

What one can see in Figure 8a is that f_m is equal to zero in the wet spot and increases slowly for points inside the turbid ring. This observation indicates that polymer diffusion began in this region of the film. Although the film has a foam-like structure in the turbid ring, local contact within clusters of particles in the foam allows for some polymer interdiffusion to occur. The extent of diffusion increases more rapidly in the dried edge of the film. Here almost all of the particles are in contact. There is more interfacial area available for diffusive mixing of polymer molecules between adjacent cells. Close to the edge of the film, for a spot that was dry for 84 min, the value of f_m reached 0.35.

A similar process is seen for the two-component latex film with the oligomer in its −COOH form. Some diffusion occurred within the foam structure at the edge of the wet spot, but the rate of diffusion increased markedly in the dry film. Here $f_m \approx 0.6$ at the far edge of the film, dry for 84 min. These results confirm that the oligomer acts as a plasticizer to increase the rate of polymer diffusion in the dry film.

When the oligomers were neutralized by ammonia (Figure 8c) or sodium hydroxide (Figure 8d), there was no observable compaction front. It is likely that ions associated with the hydrophilic shell of these core−shell particles led to more effective moisture retention at the edge of the drying front than in films formed from two-component latex nanoparticles not treated with base. Instead of a foam structure containing air voids, it is more likely that the hydrophilic shells merge into a continuous hydrophilic membrane.

Once the turbid wet spots seen in Figure 7 disappeared, the newly dried films were transparent. But upon aging at room temperature for a week, the film containing the oligomer neutralized with NaOH became hazy. The other films remained clear. To test if haziness was a consequence of moisture present in the film, we measured the equilibrium moisture content of the four types of films described in Figure 7 following drying at room temperature and 35% RH. The film formed from the core polymer itself lost 1.1 wt % upon exhaustive drying. The two-component latex films with the carboxylated oligomer and with the oligomer in the form of the NH_4^+ salt contained 1.7 wt % moisture, whereas the film containing the Na^+ salt of the oligomer contained 2.7 wt % moisture. Even after heating overnight at 100 °C, this film remained cloudy. In our discussion above of particle morphology based upon the energy transfer experiments described in Figure 5, we showed that the sodium salt of the oligomer had only limited miscibility with the core polymer. A further demonstration of the limited miscibility of these two materials is shown in Figure S10 (Supporting Information). Thus it is likely that the haziness that developed in this two-component film is a consequence of growth in size of the phase-separated domains to the point that light scattering became important.

As mentioned in the Introduction, our experimental design for these experiments was based upon the idea that the neutralized oligomer would form a hydrophilic membrane that in turn would retard the final stages of drying and delay the onset of coalescence. The data in Figure 8 provide quantitative information to test this hypothesis. The striking feature of these results is that the fraction of mixing remains negligible within approximately 1.5 mm distance from the drying front into the apparently dry film. For both ammonia and NaOH, the first point where we found an increase in f_m was approximately 1.5 mm from the drying front. While this distance seems small, it corresponds to 30 min since the passage of the drying front. In other words, although these films appear transparent in this region and particle packing has expelled all the voids and light scattering inhomogeneities, there is no measurable diffusive mixing between labeled polymers in the adjacent cells. Taking the onset of polymer diffusion across the interparticle boundary as the onset of coalescence,[12] we find that the presence of neutralized oligomer in the nanoparticles delays coalescence by half an hour at 22 °C and 35% RH.

As described by Chevalier et al., coalescence is a consequence of the breakup of hydrophilic membranes in latex films, a process analogous to the inversion of an oil-in-water emulsion to a water-in-oil emulsion. With the core polymer of adjacent cells in contact, polymer diffusion proceeds. Here we see striking differences between the film sample neutralized with NaOH and that neutralized with ammonia. For the films neutralized with NaOH, polymer diffusion is slow, reaching a value of only f_m = 0.15, 1 h after the passage of the drying front. While the dry films in an atmosphere of 35% RH contain some moisture, one can still imagine that the Na-carboxylate ion pairs form ionomer-like clusters that limit the extent of membrane break-up in the film. The presence of ion pairs in the film has another deleterious effect on final film properties. Films containing a large amount of metal carboxylate groups absorb significant amounts of moisture at high humidity and become mechanically weak when wet.[30] Thus the advantages gained from retarded coalescence in terms of a potential for enhanced open time are offset by poor water resistance of the final films.

The situation is different in the films neutralized with ammonia. While there is the same 30 min retardation of coalescence as in the films neutralized with NaOH, there is a pronounced increase in the rate of polymer diffusion once the film is dry. There is a jump in the extent of mixing at a distance corresponding to 43 min after the passage of the drying front, followed by a growth in f_m that resembles the growth rate in Figure 8b for the oligomer in the −COOH form. This behavior is consistent with the idea that when sufficiently dry, the NH_4^+−COO^- ion pairs dissociate to regenerate protonated −COOH groups as NH_3 evaporates from the film. The data in Figure 8c provide the important and useful suggestion that this process occurs as a discrete step in the drying process, in the range of 30−40 min after passage of the drying front for this system at 22 °C and 35% RH.

SUMMARY

We described the synthesis and the characterization of two-component polymer nanoparticles designed for coatings applications. The particles contain 50 wt % of a high molecular weight (high-M) copolymer of butyl acrylate (BA) and methyl methacrylate (MMA) (55:45 w/w, T_g = 6.8 °C) with $M_w \approx 1 \times 10^5$ and M_w/M_n = 2.5 as well as an equal weight of a methacrylic acid (MAA)-rich oligomer ($M_n \approx 2800$, M_w/M_n = 2.4), a copolymer of BA, MMA, MAA, and sufficient styrene to render the polymer insoluble in water when fully neutralized. For FRET experiments, we synthesized analogous samples labeled either with 1 mol % of phenanthrene (Phe) as a donor dye (D-) or 0.6 mol % 4-(*N*,*N*-dimethylaminobenzophenone) (NBen) as the acceptor dye (A-). Experiments with D-labeled oligomer and A-labeled high-M polymer showed that in individual polymer nanoparticles, with a diameter of ca. 140 nm, the acid-rich oligomer is molecularly mixed with the high-M polymer. In base, at pH of 11, phase separation occurs to form a core−shell structure, accompanied by a small increase in particle diameter (to ca. 160 nm). FRET studies show that the morphology transition occurs in minutes and is reversible with a change in pH.

Experiments with films formed from a mixture of high-M polymer labeled with both D and A show that the presence of oligomer in the −COOH form strongly accelerates the diffusion of polymer molecules across the boundaries formed by the particles in the initially formed latex films. In films formed from the two-component nanoparticles neutralized with one equivalent of base (NH_3 or NaOH), transparent latex films form upon drying, but coalescence, as monitored by the onset of

interparticle polymer diffusion, is retarded by 30 min at 22 °C and 35% RH. Interparticle adhesion should be weak in these transparent but not-yet-coalesced films. These are the conditions that should lead to enhanced open time for paints based on these nanoparticles. What is special about this experimental design for films formed from the ammonia-neutralized particles is the combination of two effects: retardation of coalescence, followed at later stages of drying by ammonium salt dissociation to reform the oligomer in its acid form. In this form it promotes intercellular diffusion of high-M polymer, the step that leads to mechanical strength in latex films.

■ ASSOCIATED CONTENT

Supporting Information. Materials and methods used for the synthesis of dispersions; description of methods and instrumentation used to characterize dispersions and dispersion polymers including: fluorescence resonance energy transfer measurements, dynamic light scattering measurements, differential scanning calorimetry measurements, capillary hydrodynamic fractionation (CHDF) measurements, gel permeation chromatography (GPC), NMR measurements, titration experiments; details and description of fluorescence data analysis and Monte Carlo simulations; and plots of Φ_{ET} of the dispersion of the doubly labeled nanoparticles at different pH, Φ_{ET} values for aqueous dispersions and for films cast from dispersions to which various amount of base had been added, values of the apparent diffusion coefficient D_{app} vs f_m for the mixtures described in Figure 7. These materials are available free of charge via the Internet at http://pubs.acs.org.

■ AUTHOR INFORMATION

Corresponding Author
mwinnik@chem.utoronto.ca

■ ACKNOWLEDGMENT

The authors thank Rohm and Haas Co. (now Dow Advanced Materials), Rohm and Haas Canada, and NSERC Canada for their support of this research. M.S. thanks the Province of Ontario for an Ontario Graduate Scholarship in Science and Technology (OGSST).

■ REFERENCES

(1) Kumar, A.; Srivastava, A.; Galaev, I.; Mattiasson, B. *Prog. Polym. Sci.* **2007**, *32*, 1205–1237.
(2) Dimitrov, I.; Trzebicka, B.; Müller, A. H. E.; Dworak, A.; Tsvetanov, C. B. *Prog. Polym. Sci.* **2007**, *32*, 1275–1343.
(3) Zhang, Q.; Li, H.; Poh, M.; Xia, F.; Cheng, Z.; Xu, H.; Huang, C. *Nature* **2002**, *419*, 284–287.
(4) Raemdonck, K.; Demeester, J.; De Smedt, S. *Soft Mater.* **2009**, *5*, 707–715.
(5) Martins, A.; Alves, C.; Kasper, F.; Mikos, A.; Reis, R. *J. Mater. Chem.* **2010**, *20*, 1638–1645.
(6) Puzzo, D.; Arsenault, A.; Manners, I.; Ozin, G. *Angew. Chem., Int. Ed.* **2009**, *48*, 943–947.
(7) Pelton, R. *Adv. Colloid Interface Sci.* **2000**, *85*, 1–33.
(8) (a) Hoare, T.; Pelton, R. *Macromolecules* **2004**, *37*, 2544–2550. (b) Bhattacharya, S.; Eckert, F.; Boyko, V.; Pich, A. *Small* **2007**, *3*, 650–657.
(9) Oh, J. K.; Drumright, R.; Siegwart, D. J.; Matyjaszewski, K. *Prog. Polym. Sci.* **2008**, *33*, 448–477.
(10) Overbeek, A.; Buckmann, F.; Martin, E.; Steenwinkel, P.; Annable, T. *Prog. Org. Coat.* **2003**, *48*, 125–139.
(11) Overbeek, A. *J. Coat. Technol. Res.* **2010**, *7*, 1–21.
(12) (a) Chevalier, Y.; Pichot, C.; Graillat, C.; Joanicot, M.; Wong, K.; Maquet, J.; Linder, P.; Cabane, B. *Colloid Polym. Sci.* **1992**, *270*, 806–821. (b) Rharbi, Y.; Boue, F.; Joanicot, M.; Cabane, B. *Macromolecules* **1996**, *29*, 4346–4359.
(13) Lau, W. *Macromol. Symp.* **2002**, *182*, 283–289.
(14) (a) Gan, D.; Lyon, L. *J. Am. Chem. Soc.* **2001**, *123*, 8203–8209. (b) Kietzke, T.; Neher, D.; Kumke, M.; Ghazy, O.; Ziener, U.; Landfester, K. *Small* **2007**, *3*, 1041–1048.
(15) Khokhlow, A.; Starodubtzev, S.; Vasilevskaya, V. *Adv. Polym. Sci.* **1993**, *109*, 123–175.
(16) Philippova, O.; Hourdet, D.; Audebert, R.; Khokhlov, A. *Macromolecules* **1997**, *30*, 8278–8285.
(17) Liu, Y.; Haley, J.; Deng, K.; Lau, W.; Winnik, M. *Macromolecules* **2007**, *40*, 6422–6431.
(18) Oh, J.; Wu, J.; Winnik, M.; Craun, G.; Rademacher, J.; Farwaha, R. *J. Polym. Sci., Part A: Polym. Chem.* **2002**, *40*, 3001–3011.
(19) O'Connor, D. V.; Phillips, D. *Time-Correlated Single Photon Counting*; Academic Press, New York, 1984.
(20) We made many attempts to obtain TEM images that would allow us to visualize the morphology of the polymer nanoparticles. None of these experiments were informative. These included attempts to stain the particles with uranyl acetate or cesium hydroxide prior to or after casting samples onto TEM grids. Unfortunately, the particles studied here are extremely soft at room temperature, and it is difficult to keep them intact when preparing the TEM grids. In addition, these polymers appeared to be very sensitive to damage when exposed to the electron beam. Attempts to use a cryo-holder to image samples at −120 °C for grids prepared at room temperature showed only fused pancake-like structures.
(21) Kawaguchi, S.; Yekta, A.; Winnik, M. A. *J. Colloid Interface Sci.* **1995**, *176*, 362–369.
(22) Helfand, E.; Tagami, Y. J. *Chem. Phys.* **1972**, *56*, 3592–3601.
(23) (a) Schillen, K.; Yekta, A.; Ni, S.; Farinha, J.; Winnik, M. *J. Phys. Chem. B* **1999**, *103*, 9090–9103. (b) Rharbi, Y.; Yekta, A.; Winnik, M.; DeVoe, R.; Barrera, D. *Macromolecules* **1999**, *32*, 3241–3248.
(24) Tronc, F.; Liu, R.; Winnik, M. A.; Eckersley, S. T.; Rose, G. D.; Weishuhn, J. M.; Meunier, D. M. *J. Polym. Sci., Part A: Polym. Chem.* **2002**, *40*, 2609–2625.
(25) Soleimani, M.; Haley, J. C.; Lau, W.; Winnik, M. A. *Macromolecules* **2010**, *43*, 975–985.
(26) (a) Haley, J. C.; Liu, Y.; Winnik, M. A.; Demmer, D.; Haslett, T.; Lau, W. *Rev. Sci. Instrum.* **2007**, *78*, No. 084101. (b) Haley, J.; Liu, Y.; Winnik, M.; Lau, W. *J. Coat. Technol. Res.* **2008**, *5*, 157–168.
(27) Ma, Y.; Davis, H.; Scriven, L. *Prog. Org. Coat.* **2005**, *52*, 46–62.
(28) Joanicot, M.; Wong, K.; Cabane, B. *Macromolecules* **1996**, *29*, 4976–4984.
(29) (a) Kim, Y.; Wool, R. *Macromolecules* **1983**, *16*, 1115–1120. (b) Wool, R.; Oconnor, K. *J. Appl. Phys.* **1981**, *52*, 5953–5963.
(30) Feng, J.; Winnik, M. A. *Macromolecules* **1997**, *30*, 4324–4331.